

# **SEISMIC SENSING WITH DEPLOYED OPTICAL FIBERS**

by

**THOMAS SUBAK**

**UNDERGRADUATE RESEARCH OPPORTUNITY PROGRAMME  
IN SCIENCE**

Project Report

**DEPARTMENT OF PHYSICS**

**NATIONAL UNIVERSITY OF SINGAPORE**

**2022**

Supervisor:

Professor Christian Kurtsiefer

## Acknowledgments

I would like to sincerely thank my supervisor, Professor Christian Kurtsiefer. This has been an amazing opportunity and learning experience for me, and I am incredibly grateful for it. I have thoroughly enjoyed working in the Quantum Optics group.

I would also like to thank my mentor Shi Yicheng. I truly appreciate your patience and guidance, it was a pleasure to be able to work on this project with you.

Thank you to the entire Quantum Optics group, especially Hou Shun, Joel, and PK for helping me get situated. This has been a great experience, so thank you to all who helped shape it to be.

# Contents

<b>Acknowledgments</b>	<b>i</b>
<b>Abstract</b>	<b>iii</b>
<b>1 Introduction</b>	<b>1</b>
1.1 Seismic Waves . . . . .	1
1.2 Earthquakes . . . . .	2
1.3 Seismometers . . . . .	3
1.3.1 Experiment Outline . . . . .	4
<b>2 Michelson Interferometer</b>	<b>5</b>
2.1 Basic Michelson Interferometer . . . . .	5
2.2 Experimental Setup . . . . .	6
2.2.1 Interference Pattern . . . . .	7
2.2.2 Fringe Analysis . . . . .	8
2.3 Experimental Data . . . . .	9
2.4 Noise . . . . .	11
2.5 Heterodyning the Interferometer . . . . .	12
<b>3 Ocean Seismometers</b>	<b>14</b>
3.1 State of Ocean Seismometers . . . . .	14
3.1.1 Ocean-Bottom Seismometers . . . . .	15
3.1.2 Floating Seismometers . . . . .	15
3.2 Michelson Interferometer as an Ocean Seismometer . . . . .	16
<b>4 Conclusion</b>	<b>17</b>
<b>Bibliography</b>	<b>18</b>

## **Abstract**

The Earth is regularly vibrating with energy from seismic waves, which can be caused by natural tectonic movement or through high energy events on the surface. Studying these events with seismometers can be incredibly useful, but the instruments can be very expensive, especially the goal is to measure submarine seismic waves. The goal of this project is too examine how Michelson interferometry could be combined with existing fiber cables that run through the ocean in order to construct a useful seismometer. The project was able to show which properties of a Michelson interferometer could be useful in seismology and which needs the interferometers would be filling.

# Chapter 1

## Introduction

### 1.1 Seismic Waves

Seismic waves are waves that propagate through the solid medium of Earth. They range in frequency from as low as 0.1 Hz to around 100 Hz [8]. The waves behave in a similar way to most waves, propagating outwards from a source, and undergo properties such as reflection, refraction, and diffraction [21] [24]. The vibrations are used to study the Earth's surface, its interior [3], and unknown properties associated with Earth's seismicity [5]. The most popular area of study in seismology is the study of earthquakes, which occur when the Earth's lithosphere suddenly releases energy in the form of seismic waves.

There are two major types of seismic waves: body waves and surface waves. Body waves travel inside the medium of the Earth. There are two forms of body waves: compression waves and shear waves. Compression waves (also known as P-waves) are the fastest wave type, and operate through compression and expansion of the Earth. Shear waves (also known as S-waves) are transverse waves that vibrate perpendicular to the direction of the wave. These waves are slower than P-waves and are unable to travel through fluid mediums such as air, water, or molten rock [16]. Surface waves are also broken into two categories: Rayleigh waves and Love waves. Rayleigh waves cause surface vibration in an elliptical pattern, whereas Love waves move earth horizontally in a direction perpendicular to the direction of motion. Love waves are faster than Rayleigh waves, but all surface waves generally have slower velocities than body waves. Among other factors, the velocities of all seismic

waves depend greatly on the density of the medium through which they travel.

When measuring earthquakes, P-waves are the first to arrive due to their high velocity. The largest waves upon arrival are the surface waves. Since their propagation is not only slower, but also limited to just the surface, they have more energy and higher amplitudes than body waves [10]. Hence, P-waves provide the first detection, and surface waves become the largest contributor to the destruction caused by Earthquakes.

## 1.2 Earthquakes

Many of the world's most destructive natural disasters are a result of seismic activity. This activity is what causes earthquakes and tsunamis, as well as often triggering volcanic activity. These events are triggered by natural tectonic movement. While anthropogenically induced seismicity has been confirmed to happen from events such as explosions, the effects are almost exclusively low magnitude, and are not the major concern of this study.

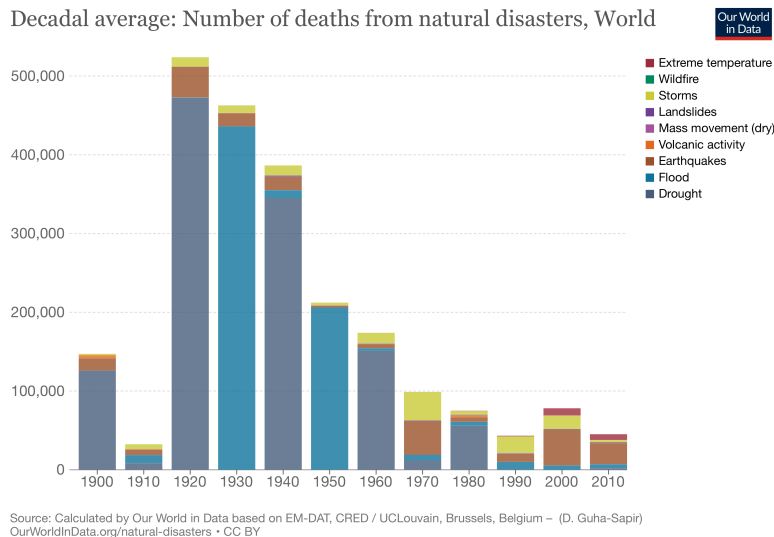


Figure 1.1: Fatalities as a result of natural disasters [15]

Seismically triggered natural disasters are responsible for tens of thousands of lives being lost each year, the global loss of tens of billions of US dollars annually, and are known to disproportionately affect poverty-stricken communities [23]. Figure

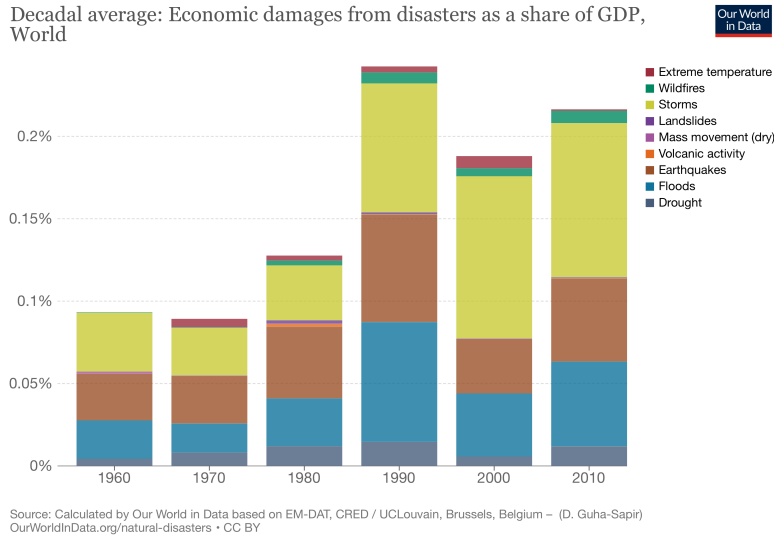


Figure 1.2: Global economic cost of natural disasters [15]

1.1 shows that as floods and droughts have become less fatal in recent decades, seismic events have become the most deadly natural disaster.

Due to this enormous cost, both financial and in the toll of human lives, many resources have been invested into earthquake seismology. To this day, scientists have never been able to predict a major earthquake before it happens. However, with continued study, more can be learned about the process, signals, and properties associated with earthquakes.

### 1.3 Seismometers

The measuring of seismic waves is done with seismographs. In a seismograph, a seismometer is used to record the ground motion which is then analyzed and combined with other data to produce a seismogram [21]. This study focuses on the seismometer component of seismographs.

Most seismometers operate using the principle of inertia. A mass on a spring hangs within a frame in such a way that the mass has a very high inertial mass. Two magnets are often used to create a magnetic field around the mass. As the wave passes through the earth, it moves the frame a great deal more than the interior mass, allowing the wave to be measured using the movement of the mass relative to

the frame [14] [9].

### 1.3.1 Experiment Outline

The vast majority of seismometers exist on land, but there do exist seismometers developed to study underwater seismic waves. These are called Ocean-Bottom Seismometers (OBS) and are currently deployed in areas across the globe [6]. There is also a theory of using existing fiber cables in an interferometer to act as an ocean seismograph, which has been well studied [22] [25] [4] [12]. The goal of this project is to examine the type of interferometer that could be used in an interferometric seismometer and analyze the potential usefulness of this type of ocean seismometer. In Chapter 2 we detail the experimental interferometer, the data collected, and discuss further adjustments that could make it a more effective seismometer. Chapter 3 contains a study of implementation possibilities and we then compare to current seismometers. Lastly, the findings are summarized and discussed in Chapter 4.

## Chapter 2

# Michelson Interferometer

### 2.1 Basic Michelson Interferometer

Interferometers combine multiple wave sources to create an interference pattern that can be used for analysis. The devices traditionally use beams of light and have become highly important due to the precise measurements that can be made based on the interference pattern produced. Of the numerous different types of optical interferometers, the Michelson interferometer is one of the most common and most popular. Created by the physicist Albert Michelson in 1887, this interferometer creates an interference pattern from a single source beam. The basic layout of a Michelson interferometer can be seen in Figure 2.1

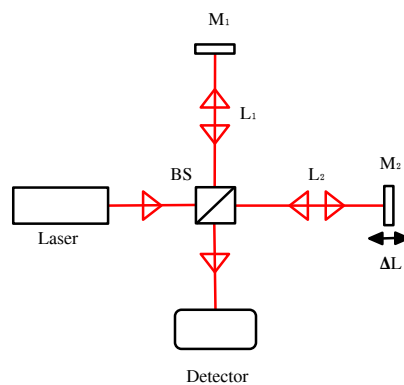


Figure 2.1: A simple Michelson interferometer. BS: Beamsplitter, M:Mirror.

## CHAPTER 2. MICHELSON INTERFEROMETER

The single beam emitted by the source is split by the 50/50 beamsplitter. Two beams then travel to two mirrors, which reflect the beams back to where they recombine and get detected. The idea of a Michelson interferometer is that the length of the two legs over which the split beam travels determines the interference pattern. The energy of the first beam is

$$E_1 = \frac{E_0}{2} e^{2ikL_1} \quad (2.1)$$

and the energy of the second

$$E_2 = \frac{E_0}{2} e^{2ik(L_2 + \Delta L)} \quad (2.2)$$

where  $k = \frac{2\pi}{\lambda}$  and  $E_0$  is the amplitude of the original beam. These equations assume that the beamsplitter has perfect 50/50 transmission/reflection and the mirrors have perfect reflection. In this simple Michelson interferometer, we can also assume that the legs are of equal length  $L_1 = L_2 = L$ . This allows us to combine equations Equation 2.1 and Equation 2.2 to form the equation

$$E_{out} = \frac{E_0}{2} e^{2ikL} (1 + e^{2ik\Delta L}) \quad (2.3)$$

This output equation is what determines the interference in the simple Michelson interferometer.

## 2.2 Experimental Setup

The experimental setup built for this project is very similar to the basic Michelson interferometer. Using a free-space optical beam, the setup has a layout that can be seen in Figure 2.2.

A 1550 nm laser was used to produce the light beam. This places the interferometer in the Infrared region of the light spectrum. To control the length of the second leg of the beam, and therefore control the path difference, the mirror M2 was placed on a movement stage. Another addition was the third mirror, M3. This was added to grant an extra degree of freedom to the setup. The ability to adjust M3 to alter the beam's path grants the user more control, and therefore more precision when positioning the beam.

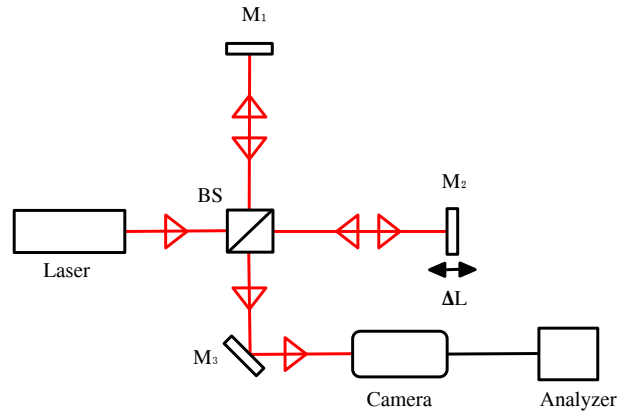


Figure 2.2: A Michelson interferometer with an added camera to capture the output beam

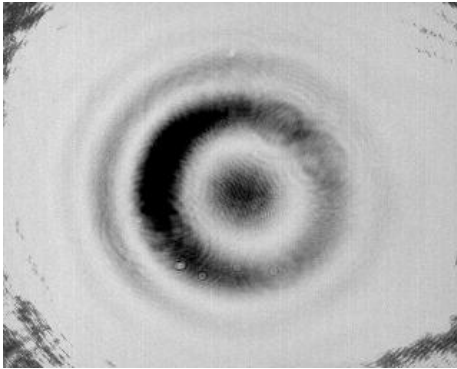


Figure 2.3: Circular fringes caused by interference of the beams

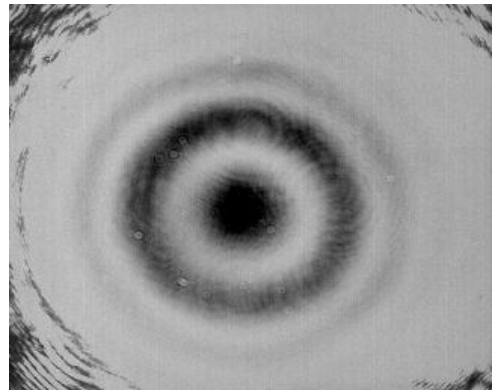


Figure 2.4: Camera images are blurred

### 2.2.1 Interference Pattern

This interferometer created the interference pattern that can be seen in Figure 2.3 and Figure 2.4. Well-aligned beams will create a fringe pattern similar to Figure 2.4, with alternating rings of light and dark fringes that correspond to constructive and destructive interference. Ideally, the pattern would have stricter fringes, possibly of the spacing seen in the corners of Figure 2.4. The blurred nature of the above figures is likely due to the intensity of the beam being too high for the camera which result in saturation of the pixels.

The pattern of the fringes is dependent on the path difference in the interferometer. Constructive interference occurs when

$$2k\Delta L = m\pi \quad (2.4)$$

for some  $m \in \mathbf{Z}^+$ . Destructive interference happens when

$$2k\Delta L = (2m + 1)\pi \quad (2.5)$$

### 2.2.2 Fringe Analysis

The distance between fringes can be measured by observing the fringe pattern. Taking a line profile of Figure 2.3 can show the fringe spacing across a vertical or horizontal line. This vertical line profile can be seen in Figure 2.5 The profile

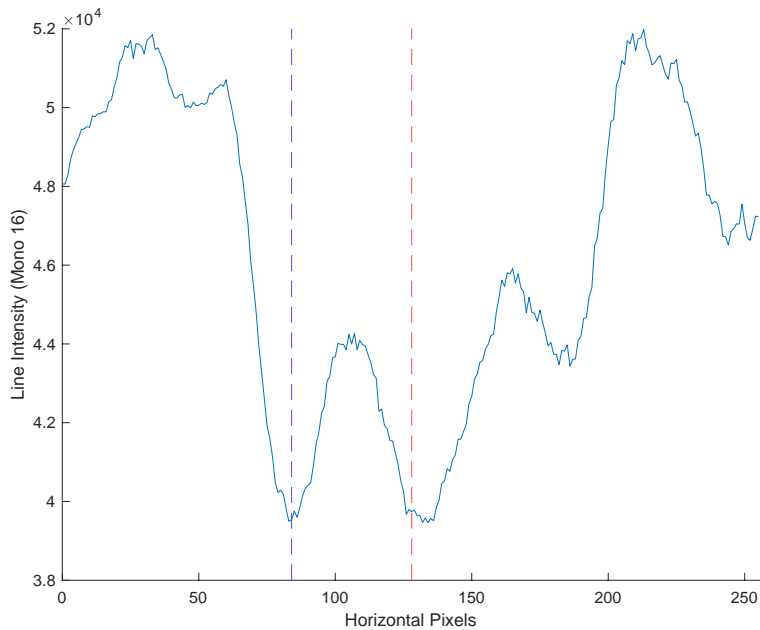


Figure 2.5: Circular fringes caused by interference of the beams

shows the total intensity at each x-coordinate of the image. This intensity is not a measurement of the maximum intensity for the interferometer however, as the beam strength was reduced to preserve the effectiveness of the camera. The camera used to capture the image was a Xenics Bobcat 320 Series. The specifications of this

device exhibit 320 x 256 pixels and a fringe distance of 20  $\mu\text{m}$ . The fringe distance is defined as the distance from the center of one pixel to the next, hence it shows the size of the pixel. Using the pixel size and vertical line profile, we can calculate the distance between consecutive dark fringes to be approximately

when

$$m_2 - m_1 = (128 - 82)20\mu\text{m} = 920\mu\text{m} \quad (2.6)$$

We find this value to be slightly less than one millimeter.

The vertical line profile can more clearly show patterns that are present in the image. For example, one can see that the two deepest minima in the graph, present at the blue and red lines, have very similar intensities. This could suggest that the maximum in between the two is the center of the pattern and a bright spot. However, one can see from Figure 2.4 that the center of the fringe pattern is dark. This implies that the central red line shows the center dark fringe, and the left blue line is showing the first destructive interference fringe outside the center. The reason the two have such similar intensities is because, as observable in the image, the fringe pattern is asymmetric and stronger towards the left side.

## 2.3 Experimental Data

Once the interference pattern was observed, the camera was then switched out of the setup to be replaced by a photodiode. As seen in Figure 2.6 this photodiode collected infrared light and transmitted the information to an oscilloscope for analysis. The photodiode converts the light collected into an electric current, and it then relays this current to the oscilloscope. The oscilloscope receives a voltage which it can then use to determine properties of the interferometer beam such as the frequency or power amplitude, then display this information.

In this experiment the oscilloscope was used to examine the relationship between the stage movement and the output power of the beam.

It can be shown that the output power depends on the phase difference [22] such that

$$P_{out} = \frac{P_{in}}{2}(1 + \cos(\phi_d)) \quad (2.7)$$

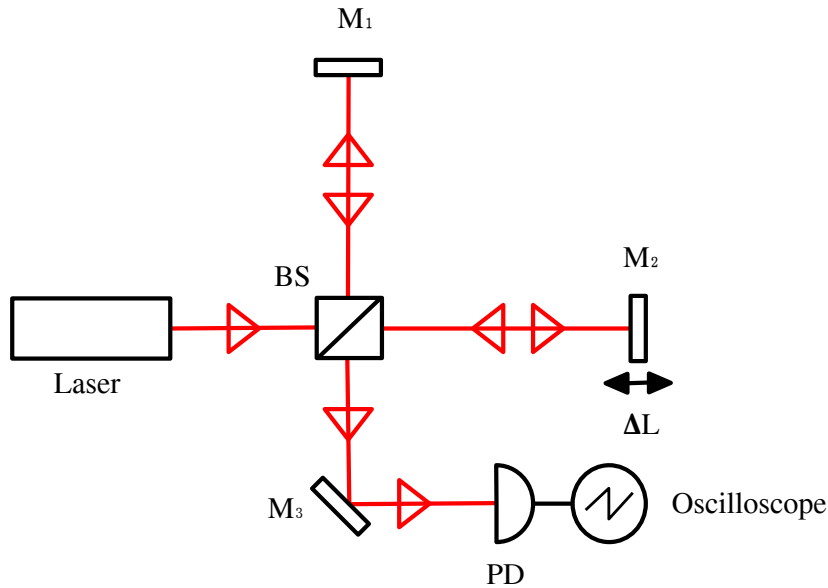


Figure 2.6: The final setup replaces the camera with a photodiode to capture the output beam

where  $\phi_d = 2k\Delta L$ .

From this equation, it can be seen that varying the leg length at a constant rate will result in a sinusoidal curve of the output power [11]. The peaks of this curve would represent constructive interference of the beam, and the troughs destructive interference. The experimental measurement of this effect can be seen in Figure 2.7. This waveform was captured by moving the stage at a constant rate and observing the data on the oscilloscope. We can see that the wave is fairly smooth, showing little effect of noise on the measurement. Another element of Figure 2.7 to note is how the troughs of the curve do not reach the x-axis. If completely destructive interference were happening in the photodiode this value should be periodically reaching zero.

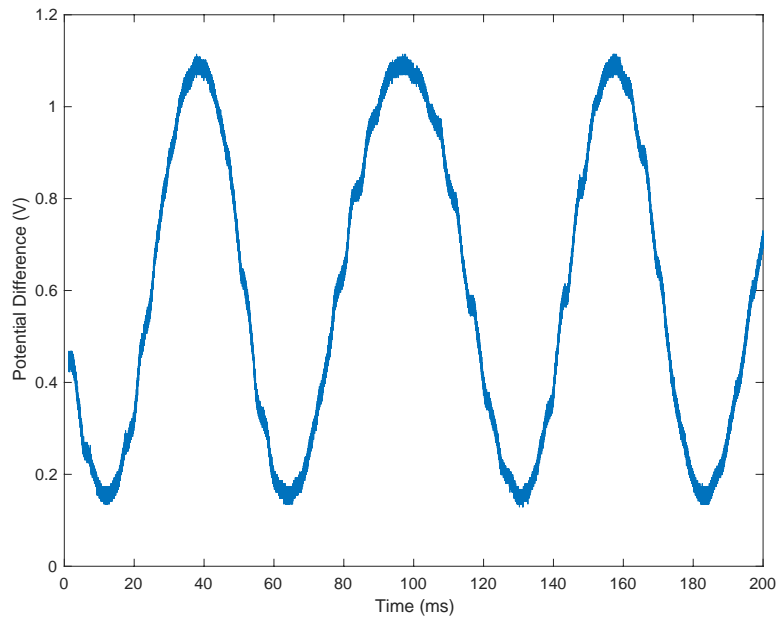


Figure 2.7: Voltage varying as the stage knob is turned at a constant rate

## 2.4 Noise

When dealing with a precision instrument such as an interferometer, it is important to address the noise involved when taking measurements. From observing Figure 2.7, a reader could assume that there is little noise involved when collecting data. If the noise did prove to be an issue in a seismometer version of this interferometer, a second photodiode could be introduced to measure the initial intensity of the beam, as was done by Watchi et al. [1]. It is true that this interferometer collects precise data on the desired scale, however it also was quite susceptible to environmental disturbance. Figure 2.8 shows the measurement of the stationary interferometer when the table on which it rests is being tapped. Each tap resulted in a voltage spike that is quite significant relative to the amplitude range of the interference. This is a factor that did not cause issues in this experiment, but would need to be addressed were this setup to be converted into an interferometric seismometer.

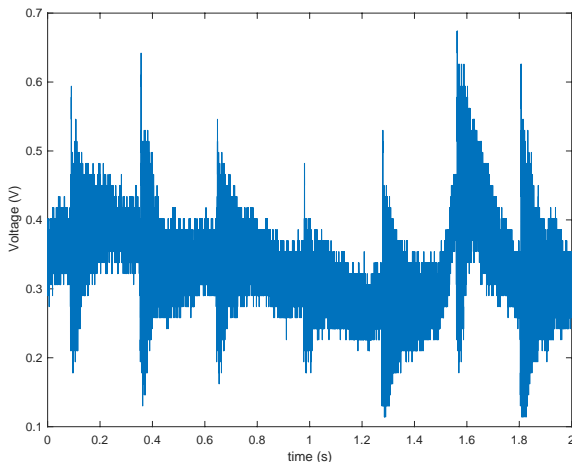


Figure 2.8: Noise produces by regular taps on the table

## 2.5 Heterodyning the Interferometer

To make an effective seismometer, the Michelson interferometer setup could be altered to form a heterodyne phasemeter as it was in previous work [22]. The first adjustment would be switching to a fiber setup, and adding a long fiber to one leg. Next steps would involve swapping the mirrors for faraday mirrors to increase sensitivity, adding an acousto-optic modulator (AOM) to shift the frequency, which would enable us to add an I/Q demodulator to finally heterodyne the setup. There could also be additions of another photodiode to reduce intensity noise and an isolator to reduce frequency noise. Since noise will no doubt be a factor in a large setup such as this, the analysis should also include a noise-correction algorithm to correct for frequency and temperature noise [7].

The I/Q demodulation is done to determine the direction of the disturbance. This is done by splitting the beam in two and performing synchronous demodulation [13]. If the power going into the modulator is

$$P = \frac{P_{in}}{2} (1 + \cos(2\Omega t + \phi_d)) \quad (2.8)$$

where  $2\Omega$  is the shift from the AOM and  $\phi_d$  is the optical phase, we can isolate  $\phi_d$  by modulating one beam with a cosine function and the other with a sine function. For example, to modulate with cosine we would use simple trigonometric identities

## CHAPTER 2. MICHELSON INTERFEROMETER

to isolate a term with  $\phi_d$

$$P = \frac{P_{in}}{2}[1 + \cos(2\Omega t)(\cos(\phi_d) - \sin(\phi_d)\sin(2\Omega t))]\cos(2\Omega t) \quad (2.9)$$

One could then distribute the cosine and through more arithmetic obtain the equation:

$$P = \frac{P_{in}}{4}[2\cos(2\Omega t) + \cos(\phi_d) + \cos(2\Omega t + \phi_d)] \quad (2.10)$$

Modulating with sine uses a similar process and results in a similar equation. They can then be passed through a low-pass filter to get rid of all functions with the  $\Omega$  term. This successfully isolates  $\phi_d$ , and results in equations

$$I = \frac{P_{in}}{4}\cos(\phi_d) \quad (2.11)$$

$$Q = \frac{-P_{in}}{4}\sin(\phi_d) \quad (2.12)$$

We can then combine equations (2.11) and (2.12) to solve for  $\phi_d$

$$Q = \frac{-I}{\cos(\phi_d)}\sin(\phi_d) \quad (2.13)$$

$$\frac{-Q}{I} = \tan(\phi_d) \quad (2.14)$$

$$\phi_d = \arctan\left(\frac{-Q}{I}\right) \quad (2.15)$$

Through I/Q demodulation, the optical phase term has been isolated outside of the cosine. This heterodyne phasemeter would be a functional addition to the simple Michelson interferometer, giving it the important ability to determine the exact value of the differential phase.

## Chapter 3

# Ocean Seismometers

### 3.1 State of Ocean Seismometers

The goal of altering this simple Michelson interferometer into a seismometer using existing fiber would have the greatest benefit in measuring oceanic seismic waves. While the theory could be used with land cables, there is a much greater need for seismic measurements in the ocean. Existing fiber cables could provide seismologists the opportunity to more accurately measure substantial areas that are currently sparsely populated with seismographs.

In the present day, roughly 1900 seismometers are deployed in the ocean, compared to about 11,500 on land [20]. This implies that less than 15% of seismometers are oceanic. This is understandable due to the relative ease of land seismometers, but evidence suggests that Earth's most important seismic activity is occurring underwater. 71% of Earth's area is covered by water. An estimated 72-82% of tsunamis are caused by underwater earthquakes [2] [19]. Additionally, the majority of the area in the Ring of Fire subduction zones is underwater, as seen in Figure 3.1:

. This area is responsible for the majority of Earth's volcanoes and an estimated 90% of earthquakes occur there [10]. For this reason, a great deal of ocean seismometers are deployed along coasts in this area. However, there is still a great deal of ocean that is poorly mapped by seismometers. Due to the large surface area and expensive nature of ocean seismometers, this is a difficult task to accomplish.

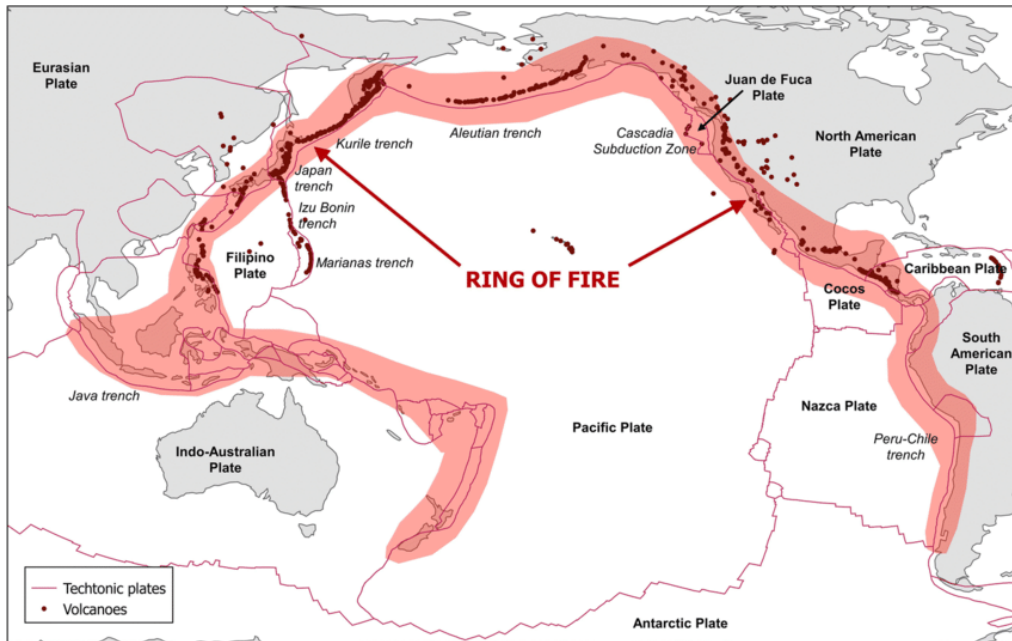


Figure 3.1: Subduction zones in the Ring of Fire (also known as the circum-Pacific belt) [17]. Subduction zones are plate boundaries in which one plate is being pushed down into the mantle by another.

### 3.1.1 Ocean-Bottom Seismometers

The majority of ocean seismometers are known as Ocean-Bottom Seismometers (OBS). They operate much in the same way that land seismometers do, but at a much higher cost. OBS often require expensive hydrophones (OBH) to accompany them. The cost of maintenance and deployment is higher due to lack of access and shorter life span. With all of those costs excluded, an OBS still costs roughly 5 times what a land-based seismometer would [20].

### 3.1.2 Floating Seismometers

A more inexpensive option compared to OBS is the floating seismometer. Floating seismometers were developed as a more cost-efficient alternative to OBS. Today, a network of devices known as MERMAID (Mobile Earthquake Recording in Marine Areas by Independent Divers) has about 50 devices deployed in the field [18]. The instruments are about a third of the price of an OBS, and float beneath the surface

automatically until they sense seismic activity and rise to the surface to transmit data. Trading ease for accuracy, the MERMAID network is much less precise than OBS. Recall that S-waves cannot propagate through fluids, which makes the MERMAID network completely unable to detect this type of wave.

## 3.2 Michelson Interferometer as an Ocean Seismometer

The basic Michelson interferometer would need to be altered and tested much further in order to serve as a functional seismometer. It can be seen from Figure 2.8 that the interferometer is incredibly sensitive to environmental noise, something that would need to be addressed when adjusting the setup. An ideal Michelson interferometer would have complete interference when the path lengths are equal. By observing figure Figure 2.7 one can see that the experimental interferometer had a minimum potential difference of about 0.1 V, which implies that the beams are slightly misaligned. It is important that the beams be well aligned in the interferometric seismometer so that every frequency of wave can be observed.

Other than those issues, however, the setup does function as a working interferometer. It is likely that with adjustments specified in Chapter 2, it could be converted into a working seismometer. Based on the data from previous experiments [22] [25] [4] [12] this is a feasible task, and a promising option for an ocean seismometer. With minimized noise and high enough precision, this type of interferometer could prove very effective at measuring both low frequency P-waves and higher frequency surface waves.

Further improvement is possible if this becomes a popular seismometer type. If the device becomes active across multiple fiber paths, a localization technique could be deployed using the different paths to determine the source [4].

Potential drawbacks to the device include difficulty implementing on existing cables, a high cost associated with the interferometer, and difficulty determining the exact behavior of the displacement wave.

## Chapter 4

# Conclusion

In this project, we constructed a simple Michelson interferometer designed to test infrared light. This included making minor alterations to a basic Michelson interferometer, constructing a photodiode circuit, and collecting data with a camera and oscilloscope.

Further, the data obtained from this interferometer setup was used to examine the possibility of a Michelson interferometer being used as a seismometer when combined with marine fiber cables. This was compared to the current state of marine seismometers and properties of seismic waves. We found that there is a definite need in the field for affordable instruments to measure seismic waves in marine areas, and the Michelson interferometric seismometer has the potential to fill that need.

# Bibliography

- [1] J. W. et al., “A review of compact interferometers”, *Review of Scientific Instruments*, vol. 89, no. 12, 2018.
- [2] B. H. et al., “Smart cables for observing the global ocean: Science and implementation”, *Frontiers in Marine Science*, vol. 6, 2019.
- [3] D. K. et al., “Sequencing seismograms: A panoptic view of scattering in the core-mantle boundary region”, *Science*, vol. 368, no. 6496, pp. 1223–1228, 2020.
- [4] G. M. et al., “Ultrastable laser interferometry for earthquake detection with terrestrial and submarine cables”, *Science*, vol. 36, pp. 486–490, 2018.
- [5] M. D. et al., “First observation of the earth’s permanent free oscillations on ocean bottom seismometers”, *Geophysical Research Letters*, vol. 44, pp. 10, 988–10, 996, 2017.
- [6] T. S. et al., “One year of seismicity recorded through ocean bottom seismometers illuminates active tectonic structures in the ionian sea (central mediterranean)”, *Frontiers in Earth Science*, vol. 9, 2021.
- [7] Y. Z. et al., “Investigation and mitigation of noise contributions in a compact heterodyne interferometer”, *Sensors*, vol. 21, no. 5788, 2021.
- [8] T. P. B. Tauzin and H. Tkalcic, “Receiver functions from seismic interferometry: A practical guide”, *Geophysical Journal International*, vol. 217, pp. 1–24, 2019.
- [9] H. Benioff, “A linear strain seismograph”, *Bulletin of the Seismological Society of America*, vol. 25, no. 4, pp. 283–309, 1935.
- [10] “Body waves inside the earth”, *USGS*,
- [11] C. Bond, “Interferometer techniques for gravitational-wave detection”, *Living Reviews in Relativity*, vol. 19, pp. 43–48, 2016.

## BIBLIOGRAPHY

- [12] T. Chang, “Fiber optic interferometric seismometer with phase feedback control”, *Optics Express*, vol. 28, no. 5, pp. 6102–6122, 2020.
- [13] K. J. Gasvik, “Optical Metrology, Chapter: Interference”, John Wiley and Sons, Ltd, 2003, pp. 37–65.
- [14] G. Gibson, “Seismic instrumentation”, *Seismology Research Centre, Royal Melbourne Institute of Technology*, 2013.
- [15] M. R. H. Ritchie, “Natural disasters”, *Our World in Data*, 2014 (Updated 2021).
- [16] S. Haldar, “Mineral Exploration (Second Edition)”, Elsevier, 2018, pp. 103–122.
- [17] D. P. I. Cheff I. Nistor, “Pedestrian evacuation modelling of a canadian west coast community from a near-field tsunami event”, *Nat Hazards*, vol. 98, pp. 229–249, 2019.
- [18] J. I. J.D. Simon F.J. Simons, “Recording earthquakes for tomographic imaging of the mantle beneath the south pacific by autonomous mermaid floats”, *Geophysical Journal International*, vol. 228, no. 1, pp. 147–170, 2022.
- [19] A. Joseph, “Tsunamis: Chapter 7 - Earthquake Detection and Monitoring for Early Warnings of Seismogenic Tsunamis”, Academic Press, 2011, pp. 109–114.
- [20] A. Lopatka, “Deploying seismometers where they’re needed most: Underwater”, *Physics Today*, 2019.
- [21] M. W. M. Stein, “An Introduction to Seismology, Earthquakes, and Earth Structure”, Blackwell, 2003.
- [22] M. N. B. Nordin, “Environmental sensing in existing fiber networks”, *National University of Singapore, Department of Physics*, 2021.
- [23] J. R. e. a. S. Hallegatte A. Vogt-Schilb, “From poverty to disaster and back: A review of the literature”, *EconDisCliCha*, vol. 4, pp. 223–247, 2020.
- [24] B. Schwartz, “An introduction to seismic diffraction”, *Advances in Geophysics*, vol. 60, pp. 1–64, 2019.

## BIBLIOGRAPHY

- [25] M. Stolarik, “New methods to seismic monitoring: Laboratory comparative study of michelson fiber-optic interferometer and pneumatic measurement systems”, *Photonics*, vol. 8, no. 147, 2021.